UDC 622.7.05

S. V. TERESHCHENKO [1], *Head of laboratory, Doctor of Engineering Sciences, tereshchenko@goi.kolasc.net.ru*
D. N. SHIBAEVA [1], *Senior Researcher, Candidate of Engineering Sciences*
P. A. SHUMILOV [1], *Researcher, Candidate of Engineering Sciences*
B. A. VLASOV [1], *Junior Researcher, Candidate of Engineering Sciences*

[1] *Mining Institute, Kola Science Center, Russian Academy of Sciences, Apatity, Russia*

EFFECT OF VIBRATING FEEDER PAN GEOMETRY ON RADIOMETRIC SEPARATOR PERFORMANCE

The article offers justifies the optimized shape for the vibrating feeder pan of a radiometric separator, which ensures the maximum travelling speed and uniform flow of ore material in the zone of radiation and recording. Three shapes of pans are discussed: rectangular, parabolic and triangular. It is found that motion of ore material along an inclined rectangular-shape pan is straight-linear. Distribution of ore particles along the width of the channel, which governs the scatter of the motion trajectories relative to the central axis of the channel, depends on the run-off point of particles from the outlet feeder. Proposed for the description of the motion trajectory of ore particles along an inclined channel of parabolic shape, the mathematical model demonstrates the curved and pendulum-wise motion of an ore particle with the attenuating amplitude. The motion of an ore particle in an inclined pan with the triangular-shape channel features the minimized scatter of motion trajectories relative to the central axis of the channel. The analysis of ore motion along vibrating feeder pans with different shape channels is carried out in Rocky DEM environment with regard to interaction of ore particles with the pan surface and with each other. The simulation modeling has proved the conclusions on the efficiency of the triangular-shape profile of the vibrating feeder pan as it ensures uniform single-row flow of ore particles along the straight-line trajectory. The triangular shape of the pan contributes to the increased travelling speed of ore particles and, accordingly, to the enhanced capacity of the separator. The radiometric separator efficiency can be increased 1.5 times by changing from the parabolic-shape channels to the triangular-shape profiles of vibrating feeder pans at the other operating conditions of radiometric separators being equal.

Keywords: *radiometric separators, handling facilities, vibrating feeder, analytical modeling, simulation modeling.*
DOI: *10.17580/em.2020.02.09*

Introduction

The ore handling system is one of the main assemblies of a radiometric separator; it ensures transfer of ore to the zone of analysis and separation into ore and gangue components.

In most cases, ore transfer from the unloading zone to the zone of radiation and recording is implemented by two series-connected facilities: an outlet vibrating feeder and a conveying vibrating feeder or a belt conveyor [1–12]. The type of a carrier facility essentially influences the separator capacity as the ore traveling speed is around of 1 m/s on the vibrating feeder pan and is three times as high on the conveyor belt. At the same time, the actual capacity of belt conveyors is lower as the high-quality concentrate production involves additional scavenging and recleaner operations [13].

In order to enhance capacity of radiometric separators with vibrating feeders, it is possible to use a multi-channel system of different-geometry channels: rectangular, parabolic and triangular [14–17]. The motion path of a body on the surface of a vibrating feeder pan is governed by the forces of gravity and friction, as well as by the pan response and environmental resistance. The pans, regardless their profiles, are made of the same material, and the dry friction force can be assumed to be constant therefore.

Justification of vibrating feeder pan shape to ensure enhanced travelling speed of rock and ore material

A body moves in the pan channel relative to the Cartesian axes; thus, projections of the force affecting this body are equal to the force components along these axes: X, Y, Z. As a result, we have the differential equations of the body motion:

$m\ddot{x} = X$; $m\ddot{y} = Y$; $m\ddot{z} = Z$.

A body moving in an inclined rectangular-shape pan is subjected to such forces as: the body weight mg; the environmental resistance proportional to the body travel speed $R = mkv$; the normal response of the pan channel plane, λ; and the friction force μx. In the first case, the law of motion is defined by the equations below:

in the X-direction: $m\ddot{x} = gm\sin\alpha - \lambda - k\dot{x}$; (1)

in the Z-direction: $m\ddot{z} = \lambda - gm\mu\cos\alpha$. (2)

Since z is always zero, the projection of motion on the axis Z is given by:

$$\lambda = gm\mu\cos\alpha. \quad (3)$$

Placing (3) in (1) produces:

$$\ddot{x} + k\dot{x} = g(\sin\alpha - \mu\cos\alpha), \quad (4)$$

where m is the mass of the body; g is the acceleration of gravity; μ is the friction factor; k – is the proportionality factor; α is the angle between the pan and the axis X; λ is the normal response of the pan channel plane.

The solution to equation (4) at $x(0) = 0$ and $\dot{x}(0) = 0$ has a form of:

$$x(t) = g(\sin\alpha - \mu\cos\alpha)(1 - e^{-kt} + t/k). \quad (5)$$

The solution to equation (2) is given by:

$$z(t) = at + b, \quad (6)$$

where a and b are constant.

Withdrawal of the time t from equations (5) and (6) allows obtaining the equation describing the body motion trajectory in the rectangular-shape pan:

$$x = g(\sin\alpha - \mu\cos\alpha)(1 - e^{-k(z-a)/b} + (z - a)/(kb)). \quad (7)$$

The theoretical inference about motion of ore in the rectangular-shape vibrating feeder pan is proved by the data of 3D Rocky DEM modeling with regard to the forces which have influence on the body, characteristics of the vibrating feeder (material and trajectory parameters, i.e. amplitude and frequency of vibrations) and of the travelling material (density, strength characteristics, i.e. Young's modulus, Poisson's ratio, shape and size distribution of particles), as well as interaction of

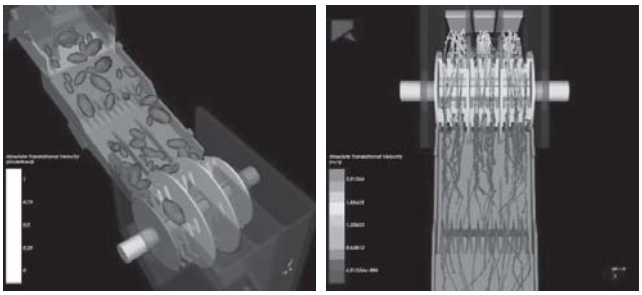

Fig. 1. Modeling of ore travel along rectangular-shape pan of vibrating feeder

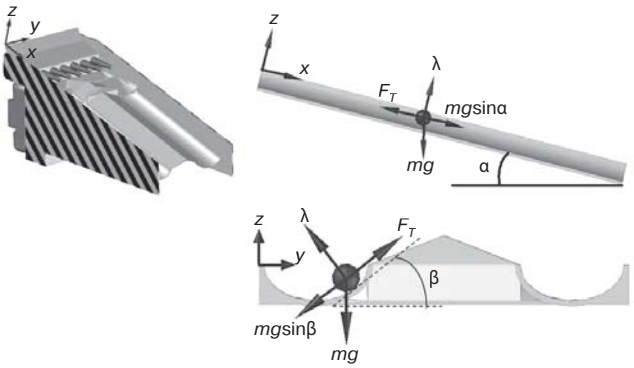

Fig. 2. Forces affecting ore particle during its travel along parabolic-shape pan

the particles with the vibrating feeder pan and with each other (**Fig. 1**). Distribution of the ore material along the width of the channel, which governs the scatter of trajectories relative to the central axis of the channel, depends on the run-off point of a particle from the outlet feeder. It is found that only 8% of the ore trajectories run along the central axis of the channel, 16.4% of the trajectories go at a distance of 2 mm, 16—at a distance of 4 mm and 59.6%—at a distance of more than 4 mm from the central axis. Departure of ore from the channel center aggravates separation. When a particle gets at the edge of the separation tool—sliding shutter, its trajectory in free fall is unpredictable, and probability of collision with other particles grows. In case of electropneumatic valve used as a separation tool, the separation efficiency decreases as well, for the same reasons.

Travel of an ore particle along a pan with a parabolic-shape channel is more complex (**Fig. 2**).

Movement of a body from the initial position at the top of the channel side (Z = H) to the opposite side by the height Z_1 with displacement along the coordinates *X* and *Y* occurs under the action of the gravity force F_g. The value of the height *Z* is found from the condition of the equality between the friction force F_{fr} and the gravity force F_g ($F_{fr} = F_g$). The pendulum motion of a body along the channel sides is preserved until its potential energy *U* vanishes. In this case when $U = 0$, the body moves along the straight-line trajectory along the pan channel.

The law of motion of a body in the pan channel in the directions of *X*, *Y* and *Z* is given by:

in the *X*-direction: $m\ddot{x} = 0$; (9)

in the *Y*-direction: $m\ddot{y} = mg(\sin(\beta(t) + \sin(\alpha)) - \mu y - k\dot{y}$; (10)

in the *Z*-direction: $m\ddot{z} = Z$, (11)

where μy is the force of friction; $k\dot{y}$ is the environmental resistance; β is the angle between the gravity force vector and the tangential to the pan channel profile.

The solution of equation (9), characterizing uniform motion of a body relative to the axis *X*:

$$x(t) = ct + d, \quad (12)$$

where *c* and *d* are constants.

We reduced equation (10) to a form of:

$$\ddot{y} + 2\varepsilon\dot{y} + \gamma y = g(\sin(\varphi(t)) + \sin(\alpha)), \quad (13)$$

where $\beta = \varphi(t)$; $k/m = 2\varepsilon$ and $\mu/m = \gamma$.

Equation (13) is a linear nonuniform equation with constant coefficients; its general solution at $\mu >> k$, initial conditions $y(0) = 0$ and $\dot{y}(0) = 0$:

$$y_{\text{general}}^{\text{nonuniform}} = \frac{1}{\gamma} - e^{-\varepsilon t}\frac{1}{\gamma}\{\sin\alpha[\cos(\delta t)\sin\alpha + 1] + \frac{\varepsilon}{\delta}\cos\alpha\sin(\delta t)\} + \frac{g\{\cos\varphi(t) + g[\dot{\varphi}(t)]^2\sin\varphi(t)\}}{\{[\dot{\varphi}(t)]^4 - [\ddot{\varphi}(t) + 2\varepsilon\dot{\varphi}(t)][1 + 2\varepsilon\dot{\varphi}(t)]\}} \quad (14)$$

where $\delta = \sqrt{\gamma - \varepsilon^2}$.

For a parabolic-shape pan at $\beta(y) = ay^2$, $z(0) = H$ and $\dot{z}(0) = 0$, the general solution of equation (11) is given by:

$$z(t) = H - \frac{\lambda}{2m}t^2[\sin\{a(\frac{1}{\gamma} - e^{-\varepsilon t}\frac{1}{\gamma}\{\sin\alpha[\cos(\delta t)\sin\alpha + 1] + \frac{\varepsilon}{\delta}\cos\alpha\sin(\delta t)\} + \frac{g\{\cos\varphi(t) + g[\dot{\varphi}(t)]^2\sin\varphi(t)\}}{\{[\dot{\varphi}(t)]^4 - [\ddot{\varphi}(t) + 2\varepsilon\dot{\varphi}(t)][1 + 2\varepsilon\dot{\varphi}(t)]\}})^2\} + \cos(\alpha)] \quad (15)$$

The solutions of (12), (14) and (15) formulate the law of motion of a body along a parabolic-shape pan. The motion in the *X* axis projection is quasi-linear; the motion in the *Y* axis projection is pendulum with attenuation, which is reflected by the presence of the exponential factor $e^{-\varepsilon t}$ in (14). The motion in the *Z* axis projection is diminishing along a parabola. Withdrawal of the time *t* from equations (12), (14) and (15) allows obtaining the equation of the body path trajectory along the pan channel:

$$z(t) = H - \frac{\lambda}{2m}\left(\frac{x-d}{c}\right)^2\left[\frac{1}{\gamma} - e^{-\varepsilon\left(\frac{x-d}{c}\right)}\frac{1}{\gamma}\left\{\sin\alpha\left[\cos\left(\delta\left(\frac{x-d}{c}\right)\right)\sin\alpha + 1\right] + \frac{\varepsilon}{\delta}\cos\alpha\sin\left(\delta\left(\frac{x-d}{c}\right)\right)\right\} + \frac{g\left\{\cos\varphi\left(\frac{x-d}{c}\right) + g\left[\dot{\varphi}\left(t\left(\frac{x-d}{c}\right)\right)\right]^2\sin\varphi\left(\frac{x-d}{c}\right)\right\}}{\left\{\left[\dot{\varphi}\left(\frac{x-d}{c}\right)\right]^4 - \left[\ddot{\varphi}\left(\frac{x-d}{c}\right) + 2\varepsilon\dot{\varphi}\left(\frac{x-d}{c}\right)\right]\left[1 + 2\varepsilon\dot{\varphi}\left(\frac{x-d}{c}\right)\right]\right\}} + \cos(\alpha)] \quad (16)$$

where *c* and *d* – const.

Figure 3 presents the Rocky DEM modeling results of motion of ore particles in a pan with parabolic-shape channels, which conform with the analytical inference on attenuating pendulum motion. However, percentage of particles traveling along the channel center is not high and is 26%; around 22% of particles move at a distance of 2 mm, 32.3%—at a distance of 4 mm and 19.7%—at a distance more than 4 mm from the central axis of the pan channel.

Travel of an ore particle in a triangular-shape channel occurs under the action of the same forces as in the previous case. The motion trajectory can be presented as two quasi-linear components: motion along the channel side inclined at an angle β to horizon and motion between the channel sides, along the central axis inclined at an angle α to horizon.

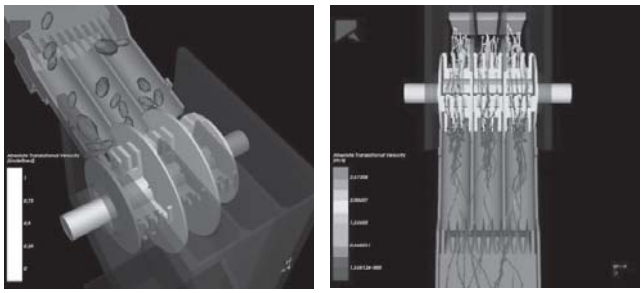

Fig. 3. Modeling of ore material travel along vibrating feeder pan with parabolic-shape channel

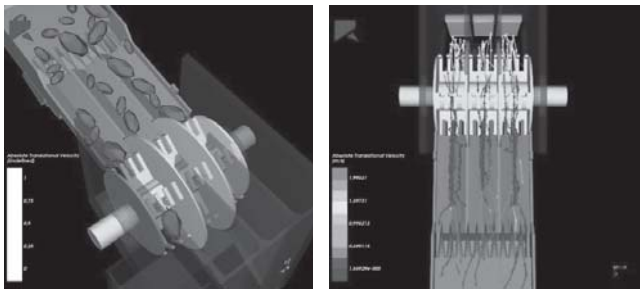

Fig. 4. Modeling of ore material travel along vibrating feeder pan with triangular-shape channel

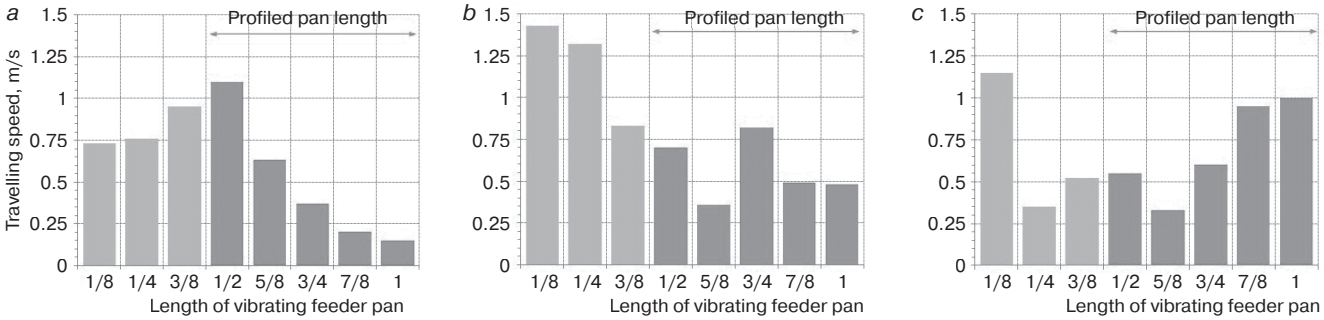

Fig. 5. Travelling speed bar charts: (*a*) rectangular-shape pan; (*b*) parabolic-shape pan; (*c*) triangular-shape pan

The equations of motion in projection on the axes *X* and *Z*:

along the axis *X*: $m\ddot{x} = mg(\sin\beta + \sin\alpha) - k\ddot{x} - \mu mg(\cos\beta + \cos\alpha)$; (17)

along the axis *Z*: $m\ddot{z} = \lambda - gm(\cos\beta + \cos\alpha)$ (18)

We reduced equation (17) to a form of:

$$\ddot{x} + 2\varepsilon\dot{x} = A, \quad (19)$$

where $A = g(\sin\beta + \sin\alpha) - \mu g(\cos\beta + \cos\alpha)$.

The solution of equation (19) at the initial condition $x(0) = 0$ and $\dot{x}(0) = 0$ is given by:

$$x(t) = g(\sin\beta + \sin\alpha) - \mu g(\cos\beta + \cos\alpha)(1 - e^{-\epsilon t} + t/k). \quad (20)$$

The law of motion in the triangular-shape pan in projection on the axis *Z:*

$$z(t) = at + b, \quad (21)$$

where *a* and *b* are the constants.

Withdrawal of the time *t* from equations (20) and (21) allows obtaining the equation of the body path trajectory along the triangular-shape pan channel:

$$x = g(\sin\beta + \sin\alpha) - \mu g(\cos\beta + \cos\alpha)(1 - e^{-k(z-a)/b} + (z - a)/(kb)). \quad (22)$$

The simulation modeling results illustrate the analytical inference (**Fig. 4**). In order to ensure the maximum approximation of the geometry of the vibrating feeder pans having channels of parabolic and triangular profiles in AutoCad modeling, the width and depth of the channels were assumed to be constant. The incline of the planes forming the triangular profile to horizon is 41°. It is found that the triangular shape of the vibrating feeder pan provides the most effective generation of a uniform ore flow: 50.7% of the motion trajectories run along the central axis, while 31.6% and 12.3% of the trajectories go at a distance of 2 and 4 mm from the central axis, respectively.

The comparative valuation of the quantitative component of the trajectory—travel along the pan profile in Rocky DEM environment shows that the maximum travel distance in the parabolic-shape channel is 5.9% shorter than the maximum travel distance in the rectangular-shape channel and 17.6% shorter than the maximum travel distance in the triangular-shape channel.

The evaluation of the travelling speeds of ore in the triangular-shape channel proves its efficiency. Minimized collision of ore particles and reduced contact area with the triangular-shape channel surface ensures enhanced travelling speed by 28.6% (0.69 m/s) as compared with the rectangular-shape channel (0.49 m/s) and by 16.9% (0.57 m/s) as against the parabolic-shape channel (**Fig. 5**).

Conclusions

Thus, the triangular-shape profile of the vibrating feeder pan shortens the travel distance of material and, accordingly, reduces the time of the material transfer to the zone of radiation and recording.

The travelling speed of ore material in the radiation and recording zone governs the radiometric separator efficiency. For this reason, an increase in the travelling speed of ore material owing to the triangular shape profile of the vibrating feeder pan can facilitate the separator performance enhancement at the other operating conditions being equal. For example, the use of the triangular-shape pans in the radiometric separators manufactured by Russian companies RADOS, KRASRADOS and TECHNOROS can improve separation capacity of size 50+20 m from 10 to 15 t/h without extra energy intake.

References

1. Tereschenko S. V., Denisov G. A., Marchevskaya V. V. Radiometric methods of testing and mineral raw material separation. Saint-Petersburg : Mining Institute of the Kola Science Centre of the Russian Academy of Sciences, 2005. 264 p.
2. Available at: http://www.rados.ru/index.php/ru/stati/82-posobie-po-rentgenoradiometricheskoj-separatsii/ (accessed: 25.02.2019).

3. Shepeta E. D., Samatova L. A., Voronova O. V. Promising trends in development of technologies for tungsten-containing ore and waste processing. *Gornyi Zhurnal*. 2018. No. 10. pp. 67–71. DOI: 10.17580/gzh.2018.10.13
4. Shepeta E. D., Samatova L. A., Alushkin I. V., Yushina T. I. Prospect of preliminary beneficiation use in the poor tungsten ores processing practice. *Non-Ferrous Metals*. 2016. Vol. 1. pp. 9–15. DOI: 10.17580/nfm.2016.01.02
5. TOMRA's mineral and ore sorting equipment for more profit. Available at: https://www.tomra.com/ru-ru/sorting/mining/ (accessed: 15.03.2020).
6. Available at: http://www.redwave.com/en/mining/ (accessed: 25.01.2019).
7. Efficiently optimise ore sorting. Available at: https://steinert-global.com/mining/ore-sorting/ (accessed: 25.01.2019).
8. Nadolski S., Samuels M., Klein B., Hart C. Evaluation of bulk and particle sensor-based sorting systems for the New Afton block caving operation. *Minerals Engineering*. 2018. Vol. 121. pp. 169–179.
9. Lessard J., Sweetser W., Bartram K. et al. Bridging the gap: Understanding the economic impact of ore sorting on a mineral processing circuit. *Minerals Engineering*. 2016. Vol. 91. pp. 92–99.
10. State-of-the-Art-Technology in Ore Mining. AT Mineral Processing. Available at: https://www.at-minerals.com/en/artikel/at_State-of-the-Art-Technology_in_Ore_Mining_1852781.html/ (accessed: 20.03.2020).
11. Separating impurities from quartz. AT Mineral Processing. Available at: https://www.at-minerals.com/en/artikel/at_Separating_impurities_from_quartz_1852565.html/ (accessed: 20.03.2020).
12. Konovalov G. N., Naumov M. E. Lump separation method. RF Patent No. RU2569528C1. MPK B03B 13/06(2006.01), B07C 5/34(2006.01). Applied:13.10.2014; published: 27.11.2015. *Byull. Izobret*. No. 33.
13. Wotruba H., Robben C. Sensor-based ore sorting in 2020. *Automatisierungstechnik*. 2020. Vol. 68(4). pp.231–238.
14. Kantsel V. A., Kantsel M. A., Mazurkevich P. A., Bogushevsky E. M. Loading-and-forming device for lump rock mass feed. RF Patent No. 2204517. MPK B65G47/19, B65G37/00. Applied: 13.07.2001; published : 20.05.2003.
15. Kantsel A. V., Danilov A. V., Tsuppinger A. A. et al. Ore separation modulus. RF Patent RU 2422210. MPK B03B 13/06, B07C 5/34. Applied: 19.03.2010; published: 27.06.2011.
16. Kantsel A. V., Mazurkevich P. A. Danilov A. V. et al. Multi-channel X-ray radiometric separator. RF Patent No. RU 2432206. MPK B03B 13/06. Applied: 29.04.2010; published: 27.10.2011, *Bulletin.* No. 30.
17. Tatarnikov A. P., Zvonarev V. N., Brodsky Yu. A. et al. Automatic ore dressing method and facility. RF Patent No. RU 2269380. MPL B03B13/00, B07C5/34. Applied: 25.05.2004; published: 10.02.2006. *Bulletin.* No. 4. EM

UDC 622.23.05

V. I. SKLYANOV[1], *Head of Mineral Mining Department, Candidate of Engineering Sciences, Associate Professor, vladimir-sklyanov@yandex.ru*
A. A. FIGURAK[2], *Senior Lecturer*
N. B. EMELINA[3], *Senior Lecturer*
A. A. EREMENKO[3,4], *Deputy Director of Science, Doctor of Engineering Science, Professor*

[1] *Norilsk State Industrial Institute, Norilsk, Russia*
[2] *Irkutsk Scientific Research Technical University, Irkutsk, Russia*
[3] *Chinakal Institute of Mining, SB RAS, Novosibirsk, Russia*
[4] *Kuzbass State Technical University, Kemerovo, Russia*

IMPROVEMENT OF WELL FLUSHING TECHNOLOGY DURING DRILLING IN PERMAFROST

The article presents the research results on flushing of wells during drilling in permafrost. The most effective flushing method is the use of drill fluids added with various antifreeze agents. In order to reduce the time spent on the implementation of this method of well flushing, as well as to prevent thawing and collapse of rocks in unstable intervals of wells, before the addition of antifreeze agents, the drill fluid is cooled down to the desired temperature. To cool drill fluids in summer, a refrigeration machine is used. In winter period, natural cold accumulated by atmospheric air is used for cooling. The drill fluid is cooled by any known method, including simplified approaches without using of complex and energy-consuming compressor refrigeration machines, by air heat exchangers blown with cold air. The proposed method involves the negative temperature mode of flushing and can be used when drilling wells of any purpose, diameter and length in permafrost up to 600 m thick.

Keywords: *well drilling, heat transfer, permafrost, antifreeze additives, drill fluid, negative temperature flushing.*
DOI: *10.17580/em.2020.02.10*

Drilling in permafrost is faced with specific difficulties at all stages of well construction [1–10]. These difficulties arise from the variation in thermal conditions in wells due to heat exchange between permafrost rocks and the flush fluid circulating in the wells. To prevent freezing problems when drilling in permafrost, heated process water or drill fluid are used, which often results in decohesion of permafrost, as well as in sloughing and caving-in of wells.

According to the accomplished studies, the most effective technique of well washing in such conditions is application of negative-temperature drill fluids added with antifreeze agents, including